

Superconductivity in FeSe thin films driven by the interplay between nematic fluctuations and spin-orbit coupling

Jian Kang* and Rafael M. Fernandes

School of Physics and Astronomy, University of Minnesota, Minneapolis, MN 55455, USA

The origin of the high-temperature superconducting state observed in FeSe thin films, whose phase diagram displays no sign of magnetic order, remains a hotly debated topic. Here we investigate whether fluctuations arising due to the proximity to a nematic phase, which is observed in the phase diagram of this material, can promote superconductivity. We find that nematic fluctuations alone promote a highly degenerate pairing state, in which both s -wave and d -wave symmetries are equally favored, and T_c is consequently suppressed. However, the presence of a sizable spin-orbit coupling or inversion symmetry-breaking at the film interface lifts this harmful degeneracy and selects the s -wave state, in agreement with recent experimental proposals. The resulting gap function displays a weak anisotropy, which agrees with experiments in monolayer FeSe and intercalated $\text{Li}_{1-x}(\text{OH})_x\text{FeSe}$.

In most iron-based superconductors (FeSC), superconductivity is found in close proximity to a magnetically ordered state, suggesting that magnetic fluctuations play an important role in binding the Cooper pairs [1–4]. Indeed, the fact that the Fermi surface of these materials is composed of small hole pockets and electron pockets separated by the magnetic ordering vector led to the proposal of a sign-changing s^{+-} wave state, in which the gap function has different signs in the hole and in the electron pockets. However, the recent observation of superconductivity over 70 K in monolayer FeSe brought new challenges to the field [5–14]. In contrast to the standard FeSC, no long-range magnetic order is observed in thin films or even bulk FeSe [15], and the Fermi surface of monolayer FeSe consists of electron pockets only [6, 7, 11, 16]. Since T_c in monolayer FeSe is the highest among all FeSC, the elucidation of its origin is a fundamental step in the search for higher T_c in these systems.

One of the proposed scenarios to explain the dramatic ten-fold increase of T_c in monolayer FeSe with respect to the 8 K value in bulk FeSe [17] was the strong coupling to an optical phonon mode of the SrTiO_3 (STO) substrate [16, 18, 19], which is manifested by replica bands observed in ARPES [16]. Although such a coupling can certainly enhance T_c [20–24], recent experiments indicate that the STO substrate may not be essential to achieve the high- T_c state. In particular, T_c up to 40 K was observed in electrostatically-gated films of FeSe with different thickness grown both on STO and MgO substrates [25]. Similar values of T_c were reported in FeSe coated with potassium [26, 27] and in the bulk sample $\text{Li}_{1-x}(\text{OH})_x\text{FeSe}$ [28, 29], which consists of intercalated FeSe layers. In common to all these systems is the fact that their Fermi surface consists of electron pockets only, suggesting that doping by negative charge carriers plays a fundamental role in stabilizing the high- T_c state.

Importantly, recent experiments in K-coated bulk FeSe [26] revealed that, besides shifting the chemical potential, electron-doping also suppresses the nematic order ob-

served in undoped bulk FeSe at $T_{\text{nem}} \approx 90$ K [30]. In the nematic state, whose origin remains hotly debated [31–35], the x and y in-plane directions become inequivalent and orbital order emerges. Remarkably, the highest T_c in the phase diagram of K-coated FeSe is observed near the region where T_{nem} nearly vanishes. Similarly, in the case of FeSe thin films grown on STO, nematic order is observed over a wide range of film thickness [36, 37], but not in the monolayer case [38]. These observations, combined with the absence of magnetic order in these systems, begs the question of whether nematic fluctuations can provide a sensible mechanism to explain the superconductivity of thin films of FeSe [22, 26, 39, 40].

In this paper, we show that nematic fluctuations alone favor degenerate s -wave (A_{1g}) and d -wave (B_{2g}) superconducting states in FeSe thin films. This degeneracy stems from the fact that while the two electron pockets are separated by the momentum $\mathbf{Q}_M = (\pi, \pi)$, nematic fluctuations are peaked at $\mathbf{Q}_{\text{nem}} = 0$. More importantly, the SC ground state manifold has an enlarged $U(1) \times U(1)$ degeneracy, which is very detrimental to SC, since fluctuations of one SC channel strongly suppress long-range order in the other SC channel. Remarkably, this degeneracy is removed by the sizable spin-orbit coupling (SOC) observed in these compounds [41], which lift the pairing frustration and selects s -wave over d -wave, stabilizing a SC state at higher temperatures. In thin films, the inversion symmetry-breaking (ISB) at the interface also contributes significantly to this degeneracy lifting. Interestingly, recent experiments propose that an s -wave state is realized in FeSe thin films [42]. We also find that, when the SOC and/or ISB energy scales are larger than the energy scale associated with the mismatch between the two electron pockets, a nearly isotropic gap appears at the electron pockets, whose angular dependence agrees with ARPES and STM measurements in FeSe thin films [26, 43] and intercalated $\text{Li}_{1-x}(\text{OH})_x\text{FeSe}$ [44].

Microscopic model We start with the full five-orbital tight-binding model in the 1-Fe Brillouin zone

and project it on the subspace of the d_{xz} , d_{yz} , and d_{xy} orbitals, which give the largest contribution to the Fermi surface. In particular, while the X electron pocket centered at $\mathbf{Q}_X = (\pi, 0)$ has d_{yz}/d_{xy} orbital content, the Y electron pocket centered at $\mathbf{Q}_Y = (0, \pi)$ has d_{xz}/d_{xy} content (see Fig. 1a). Following Ref. [45], we expand the projected tight-binding matrix in powers of the momentum measured relative to \mathbf{Q}_X and \mathbf{Q}_Y . Defining two spinors corresponding to each electron pocket:

$$\begin{aligned}\Psi_X(\mathbf{k}) &\approx (d_{yz}(\mathbf{k} + \mathbf{Q}_X), d_{xy}(\mathbf{k} + \mathbf{Q}_X))^T \\ \Psi_Y(\mathbf{k}) &\approx (d_{xz}(\mathbf{k} + \mathbf{Q}_Y), d_{xy}(\mathbf{k} + \mathbf{Q}_Y))^T\end{aligned}\quad (1)$$

the non-interacting Hamiltonian is written as $\mathcal{H}_0 = \sum_{\mathbf{k}, i=X,Y} \Psi_i^\dagger(\mathbf{k}) \hat{H}_i(\mathbf{k}) \Psi_i(\mathbf{k})$ where \hat{H}_i are 2×2 matrices in spinor space (see the supplementary material SM). The B_{2g} nematic order parameter is described by the bosonic field ϕ_q , with $q = (\Omega_n, \mathbf{q})$, whereas the nematic fluctuations are given by the nematic susceptibility $\chi_{\text{nem}}(\mathbf{q}, \Omega_n)$. For our analysis, it is not necessary to specify the origin of the nematic order parameter, but rather how it couples to the electronic states. As discussed in Ref. [46], there are two possible nematic couplings: λ_1 , which couples ϕ_q to the onsite energy difference between the d_{xz} and d_{yz} orbitals, and λ_2 , which couples ϕ_q to the hopping anisotropy between nearest-neighbor d_{xy} orbitals (see Fig. 1b):

$$\mathcal{H}_{\text{int}} = \sum_{\mathbf{q}, i=X,Y} \phi_{-\mathbf{q}} \Psi_i^\dagger(\mathbf{k}) \hat{\lambda}_i^{\text{nem}} \Psi_i(\mathbf{k} + \mathbf{q}) \quad (2)$$

with $\hat{\lambda}_i^{\text{nem}} = \pm \text{diag}(\lambda_1, \lambda_2)$, where the plus (minus) sign refers to $i = X$ ($i = Y$). Here, we focus on the effect of short-ranged frequency independent nematic fluctuations and approximate $\chi_{\text{nem}}(\mathbf{q}, \Omega_n)$ by its zero momentum and zero frequency value. The first approximation is justified due to the smallness of the electron pockets, whereas the second one is reasonable as long as the system is not too close to a nematic quantum critical point [40, 47, 48]. Note that renormalization-group calculations on a related microscopic model support the idea that the disappearance of the central hole pockets suppresses nematic order [32].

Superconducting instability We decompose the pairing states in terms of the different irreducible representations of the space group of the FeSe plane, $P4/nmm$ (see Ref. [45] and the SM), and focus on the two leading pairing channels, which belong to the singlet s -wave (A_{1g}) and d -wave (B_{2g}) symmetry representations [49]:

$$\Psi_X^T \begin{pmatrix} \Delta_1 & 0 \\ 0 & \Delta_2 \end{pmatrix} \otimes i\sigma_2 \Psi_X \pm \Psi_Y^T \begin{pmatrix} \Delta_1 & 0 \\ 0 & \Delta_2 \end{pmatrix} \otimes i\sigma_2 \Psi_Y \quad (3)$$

where the plus (minus) sign refers to s -wave (d -wave) pairing. The gaps Δ_1 and Δ_2 correspond to intra-orbital

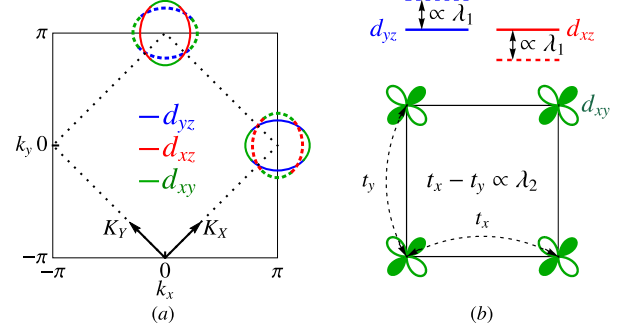


FIG. 1: (a) Fermi surface (FS) of a thin film of FeSe, consisting only of electron pockets, in the unfolded (solid lines) and folded (dotted lines) Brillouin zones. The color around the FS indicates the orbital that contributes the largest spectral weight. (b) The two different nematic couplings: λ_1 couples to the on-site energy difference between the d_{xz} and d_{yz} orbitals, whereas λ_2 couples to the anisotropic hopping between nearest-neighbor d_{xy} orbitals.

pairing within the d_{xz}/d_{yz} orbitals and d_{xy} orbitals, respectively. Δ_1 and Δ_2 are found via the gap equations:

$$\eta \hat{M} = \chi_{\text{nem}} T \sum_{n, \mathbf{k}} \left(\hat{\lambda}_i^{\text{nem}} \right)^T \hat{G}_{-k, i}^T \hat{M} \hat{G}_{k, i} \hat{\lambda}_i^{\text{nem}} \quad (4)$$

where η is the SC eigenvalue, $\hat{M} = \begin{pmatrix} \Delta_1 & 0 \\ 0 & \Delta_2 \end{pmatrix}$, and $\hat{G}_{p, i}^{-1} = i\omega_n - \hat{H}_i(\mathbf{p})$. The SC transition temperature is obtained when $\eta = 1$. Hereafter, we set the value of $(\lambda_1^2 + \lambda_2^2) \chi_{\text{nem}}$ to yield $T_c = 5\text{meV}$ when $\lambda_2 = 0$.

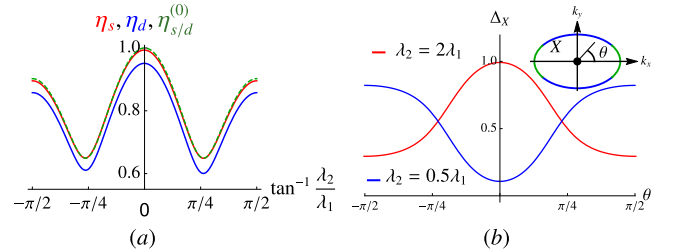


FIG. 2: (a) The eigenvalue η of the gap equation (4) as function of the ratio between the two nematic couplings λ_2/λ_1 . Without SOC or ISB, the s -wave and d -wave solutions have the same eigenvalue (dashed green curve, $\eta_{s/d}^{(0)}$). The presence of SOC or ISB removes this degeneracy, making s -wave (red curve, η_s) the leading pairing instability and d -wave (blue curve, η_d) the subleading one. (b) Normalized SC gap along the X electron pocket as function of the angle θ for different values of λ_2/λ_1 .

Solution of the gap equations reveals that for all ratios of the nematic coupling constants λ_1 and λ_2 , the superconducting instabilities in the s -wave and d -wave channels are always degenerate, as shown in Fig. 2a. Although

the intra-orbital gaps Δ_1 and Δ_2 are isotropic, the gaps projected onto the Fermi pockets, Δ_X and Δ_Y , acquire an angle-dependence due to the orbital content of the Fermi pockets. To illustrate this behavior, Fig. 2b shows Δ_X as function of the polar angle θ . When $\lambda_1 > \lambda_2$, nematic fluctuations couple mainly to the d_{xz}/d_{yz} orbitals; as a result, Δ_X is proportional to the spectral weight of the d_{xz}/d_{yz} orbital on the X pockets, which is maximum around $\theta = \pm\pi/2$ (see Fig. 1a). Consequently, Δ_X reaches its maximum at $\theta = \pm\pi/2$ and its minimum at $\theta = 0, \pi$. Conversely, for $\lambda_1 < \lambda_2$, the gap is maximum at $\theta = 0, \pi$, where the spectral weight of the d_{xy} orbital on the X pocket is maximum. Recent ARPES experiments in FeSe suggest that λ_1 and λ_2 are comparable [50].

In terms of the averaged gaps Δ_X and Δ_Y , the s -wave and d -wave solutions correspond to $\Delta_s = \frac{1}{2}(\Delta_X + \Delta_Y)$ and $\Delta_d = \frac{1}{2}(\Delta_X - \Delta_Y)$. Using this notation, the degeneracy between s and d can be understood as a consequence of the fact that nematic fluctuations, peaked at $\mathbf{Q}_{\text{nem}} = 0$, do not couple the gaps at the X and Y pockets, since they are displaced by the momentum $\mathbf{Q}_M = \mathbf{Q}_X + \mathbf{Q}_Y = (\pi, \pi)$. This suggests an enlarged $U(1) \times U(1)$ degeneracy of the SC ground state manifold, corresponding to two decoupled SC order parameters. To investigate the robustness of this enlarged degeneracy, we went beyond the linearized gap equations and computed the superconducting free energy to quartic order in the gaps (see SM), obtaining:

$$F_{SC} = a(|\Delta_X|^2 + |\Delta_Y|^2) + \frac{u}{2}(|\Delta_X|^4 + |\Delta_Y|^4) \quad (5)$$

This form confirms that Δ_X and Δ_Y remain decoupled to higher orders in F_{SC} . The consequences of this enlarged $U(1) \times U(1)$ degeneracy are severe: going beyond the mean-field approximation of Eq. (4), fluctuations of one SC channel suppress long-range order in the other channel, i.e. $T_{c,s} - T_{c,0} \propto -\langle \Delta_d^2 \rangle$. Such a pairing frustration is therefore detrimental to SC [51–54], suggesting that nematic fluctuations alone do not provide an optimal SC pairing mechanism in this system. Interestingly, previous investigations of SC induced by nematic fluctuations in different models also found nearly-degenerate states [39, 55].

Spin-orbit coupling (SOC) and Inversion symmetry-breaking (ISB) The analysis above neglected a key property of the crystal structure of the FeSe plane: Because of the puckering of the Se atoms above and below the Fe square lattice, the actual crystallographic unit cell contains 2 Fe atoms. As a result, in the 2-Fe Brillouin zone (the folded BZ), the momentum $\mathbf{Q}_M = (\pi, \pi)$ becomes $\tilde{\mathbf{Q}} = 0$ (hereafter the tilde denotes a wave-vector in the folded BZ). Thus, the two electron pockets become centered at the same momentum $\tilde{\mathbf{Q}} = (\pi, \pi)$ and overlap, as shown by the dashed lines in Fig. 1a.

This property opens up the possibility of coupling the Δ_X and Δ_Y gaps and removing the enlarged $U(1) \times U(1)$

degeneracy. At the non-interacting level, this is accomplished by the atomic spin orbit coupling $\lambda_{\text{SOC}} \mathbf{S} \cdot \mathbf{L}$, which couples the d_{xz} (d_{yz}) orbital associated with the Y (X) pocket to the d_{xy} orbital associated with the X (Y) pocket [46]:

$$\mathcal{H}_{\text{SOC}} = \frac{i}{2} \lambda_{\text{SOC}} \sum_{\mathbf{k}} \Psi_Y^\dagger (\tau_+ \otimes \sigma_1 + \tau_- \otimes \sigma_2) \Psi_X + h.c. \quad (6)$$

where τ and σ are Pauli matrices in spinor and spin spaces, respectively. While in the normal state the SOC splits the two overlapping elliptical electron pockets centered at $\tilde{\mathbf{Q}} = (\pi, \pi)$ into inner and outer pockets (see Fig. 3a and the ARPES data of [41]), in the SC state it couples the gaps Δ_X and Δ_Y . For λ_{SOC} small compared to ϵ_m – the energy scale associated with the mismatch between the X and Y electron pockets – this coupling is given perturbatively by the Feynman diagram of Fig. 3b, which gives the following contribution to the SC free energy of Eq. (5):

$$\delta F_{SC} = \gamma (\Delta_X \Delta_Y^* + h.c.) \quad (7)$$

As shown in the SM, $\gamma \propto -\lambda^2$, implying that the SOC selects the s -wave state, with Δ_X and Δ_Y of the same sign, over the d -wave state, with Δ_X and Δ_Y of opposite signs. More importantly, it lifts the $U(1) \times U(1)$ degeneracy between the two pairing states, suppressing the negative interference of one pairing channel on the other. We confirmed this general conclusion by evaluating explicitly the gap equations in the A_{1g} (s -wave) and B_{2g} (d -wave) channels, finding that $\eta_s > \eta_d$ for all values of the nematic coupling constants, as shown in Fig. 2a. Note that the SOC induces triplet components to these pairing states (see SM).

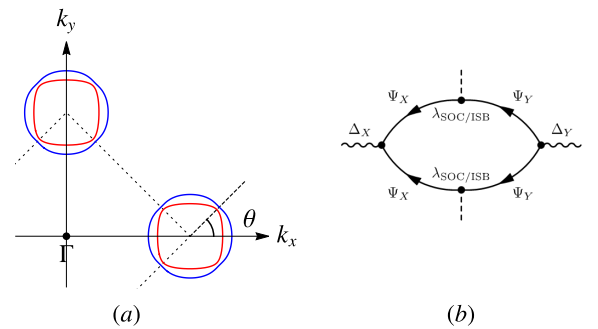


FIG. 3: (a) The Fermi surface in the presence of SOC or ISB consists of split inner (red) and outer (blue) electron pockets. (b) Feynman diagram representing the coupling between the gaps in the two electron pockets promoted by SOC or ISB. This coupling lifts the degeneracy between s -wave and d -wave.

Having established that the A_{1g} channel is the leading SC instability, we now discuss the angular dependence

of the gaps $\Delta_{i/o}$ around the inner (*i*) and outer (*o*) electron pockets. When $\lambda_{\text{SOC}} \ll \epsilon_m$, as it is apparent from Fig. 1a, the outer electron pocket consists mostly of d_{xy} orbital spectral weight, whereas the inner pocket consists mostly of d_{xz}/d_{yz} spectral weight. The d_{xz} and d_{yz} gap functions have essentially the same angular dependence as in the case without SOC, shown previously in Fig. 2b. Consequently, the gap anisotropy depends strongly on the ratio λ_1/λ_2 between the two nematic couplings. For $\lambda_1 \approx \lambda_2$, the gaps are nearly isotropic around the inner and outer pockets, whereas for $\lambda_1 < \lambda_2$ or $\lambda_1 > \lambda_2$, the gaps are anisotropic in both pockets.

The gap structure however changes dramatically in the case $\lambda_{\text{SOC}} \gg \epsilon_m$ (with both still much smaller than the Fermi energy). In this case, the two reconstructed electron pockets are fully hybridized, implying that their orbital weights are similar. As a result, the SC gaps on the inner and outer pockets are weakly anisotropic for all values of the ratio λ_1/λ_2 , whose main effect is to displace the position of the gap maxima. While for $\lambda_1 < \lambda_2$ the gap minima are located at the intersection points between the two un-hybridized electron pockets, $\theta = \pm\pi/4$, for $\lambda_1 > \lambda_2$ the gap minima are found at the intersection points (see Fig. 4). Interestingly, recent ARPES experiments in monolayer FeSe observe gap maxima at $\theta = \pm\pi/4$ [56], whereas STM measurements in the intercalated $\text{Li}_{1-x}(\text{OH})_x\text{FeSe}$ compound report gap minima at $\theta = \pm\pi/4$ [44].

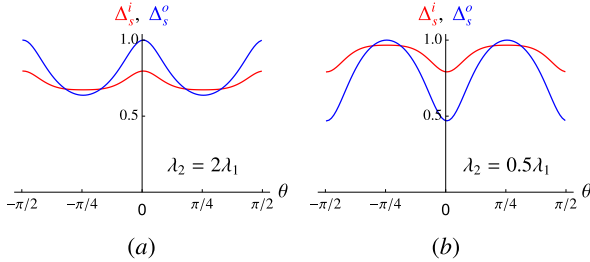


FIG. 4: Angular dependence of the SC gap along the inner (red) and outer (blue) electron pocket in the case where the SOC coupling is much larger than the electron pockets mismatch. The positions of the gap minima are controlled by λ_2/λ_1 .

Besides SOC, the inversion-symmetry breaking (ISB) at the interface of thin films also lifts the degeneracy between *s*-wave and *d*-wave in the case of FeSe thin films. In terms of the low-energy spinor states, ISB gives rise to the term [57]:

$$H_{\text{ISB}} = \lambda_{\text{ISB}} \sum_{\mathbf{k}} \Psi_X^\dagger \frac{\tau_0 + \tau_3}{2} \Psi_Y + h.c. \quad (8)$$

Similarly to SOC, λ_{ISB} hybridizes the two electron pockets and favors *s*-wave over *d*-wave, lifting the degeneracy between the two states (Fig. 3b) and enhancing the *s*-wave pairing instability. As shown in the SM, the

effect of ISB on the angular dependence of the gap functions around the inner and outer pockets is very similar to the effect of SOC. The only difference is that because ISB barely couples to the d_{xy} orbitals, the gaps remain moderately anisotropic.

So far we considered only the zero-momentum contribution of the nematic fluctuations. In general, however, $\chi_{\text{nem}}^{-1}(\mathbf{q}) = \xi_{\text{nem}}^{-2} + q^2$. Thus, although small-momentum fluctuations do not couple the *X* and *Y* pockets, leaving the *s*-wave/*d*-wave degeneracy intact, large-momentum fluctuations couple them, giving rise to their own free-energy coupling γ' in Eq. (7). As shown in the SM, however, $\gamma' \ll \gamma$, implying that the small-momentum approximation is sensible.

Besides SOC and ISB, other effects can lift the *s*-wave/*d*-wave degeneracy promoted by the dominant nematic fluctuations. For instance, magnetic fluctuations peaked at (π, π) would favor the *d*-wave state [58, 59], whereas a momentum-independent electron-phonon interaction would favor the *s*-wave state. To the best of our knowledge, no sign of (π, π) magnetic order has been observed in FeSe thin films with only electron pockets. First-principle calculations for the momentum-independent phonon coupling estimate a resulting $T_c \lesssim 1$ K [60], an energy scale that may be too small to significantly lift the degeneracy, since $T_c \approx 40$ K in FeSe thin films.

Previous works have shown that forward-scattering phonons can lead to a sizable enhancement of T_c in FeSe films grown over SrTiO₃ or BaTiO₃ [18, 20–24]. Indeed, the observation of replica band in ARPES measurements highlights the importance of this phonon mode [16]. Similarly to the nematic fluctuations studied here, forward-scattering phonons are also peaked at zero momentum, and therefore are expected to also promote degenerate *s*-wave/*d*-wave SC states [24]. In this regard, the two pairing mechanisms may cooperate to promote a robust SC state, whose degeneracy is lifted by SOC or ISB. While a detailed analysis of this problem is beyond the scope of this work, it is tempting to attribute to this cooperative effect the fact that T_c is higher in FeSe films grown over titanium oxide interfaces as compared to other types of interfaces or other FeSe-based compounds.

Summary In summary, we showed that the combined effect of nematic fluctuations and SOC/ISB favors an *s*-wave state in electron-doped thin films of FeSe, in agreement with recent experimental proposals [42]. The role played by SOC and ISB is fundamental to lift the degeneracy with the sub-leading *d*-wave state, which suppresses the onset of long-range SC order. Although nematic fluctuations are momentum-independent in our model, the gap function can acquire a pronounced angular dependence since the nematic order parameter couples differently to d_{xz}/d_{yz} and d_{xy} orbitals. Interestingly, in the regime where the SOC and ISB couplings are larger than the mismatch between the electron pockets, we obtain a

gap function whose angular dependence agrees qualitatively with measurements in monolayer FeSe and intercalated $\text{Li}_{1-x}(\text{OH})_x\text{FeSe}$. More generally, our work provides an interesting framework in which superconductivity can develop in the presence of nematic fluctuations.

We thank A. Chubukov, S. Lederer, X. Liu, A. Millis, M. Khodas, S. Kivelson, S. Raghu, D. Scalapino, M. Schüt, Y. Wang, O. Vafek, and Y. Y. Zhao for fruitful discussions. This work was supported by the U.S. Department of Energy, Office of Science, Basic Energy Sciences, under Award number de-sc0012336.

* Electronic address: jkang@umn.edu

- [1] I. I. Mazin, D. J. Singh, M. D. Johannes, M.H. Du, Phys. Rev. Lett. **101**, 057003 (2008).
- [2] P. J. Hirschfeld, M. M. Korshunov, and I. I. Mazin, Rep. Prog. Phys. **74**, 124508 (2011).
- [3] D. N. Basov and A. V. Chubukov, Nature Phys. **7**, 272 (2011).
- [4] A. V. Chubukov, Annu. Rev. Condens. Matter Phys. **3**, 5792 (2012).
- [5] Q. Y. Wang, *et al.*, Chin. Phys. Lett. **29**, 037402 (2012).
- [6] D. F. Liu *et al.*, Nat. Commun. **3**, 931 (2012).
- [7] S. L. He *et al.*, Nat. Mater. **12**, 605 (2013).
- [8] S. Tan *et al.*, Nat. Mater. **12**, 634 (2013).
- [9] W. H. Zhang, *et al.*, Chin. Phys. Lett. **31**, 017401 (2014).
- [10] J.-F. Ge, Z.-L. Liu, C. Liu, C.-L. Gao, D. Qian, Q.-K. Xue, Y. Liu, and J.-F. Jia, Nature Mater., **14**, 285 (2014).
- [11] P. Zhang, *et al.*, Phys. Rev. B **94**, 104510 (2016).
- [12] R. Peng, *et al.*, Nature Commun. **5**, 5044 (2014).
- [13] B. Lei, *et al.*, Phys. Rev. Lett. **116**, 077002 (2016).
- [14] Y. Sun, W. Zhang, Y. Xing, F. Li, Y. Zhao, Z. Xia, L. Wang, X. Ma, Q.-K. Xue, and J. Wang, Sci. Rep. **4**, 6040 (2014).
- [15] E. Pomjakushina, K. Conder, V. Pomjakushin, M. Bendele, and R. Khasanov, Phys. Rev. B **80**, 024517 (2009).
- [16] J. J. Lee, *et al.*, Nature **515**, 245 (2014).
- [17] F.-C. Hsu, *et al.*, Proc. Natl Acad. Sci. **105**, 14262 (2008).
- [18] Y.-Y. Xiang, F. Wang, D. Wang, Q.-H. Wang, and D.-H. Lee, Phys. Rev. B **86**, 134508 (2012).
- [19] Y. C. Tian, W. H. Zhang, F. S. Li, Y. L. Wu, Q. Wu, F. Sun, G. Y. Zhou, L. Wang, X. Ma, Q.-K. Xue, and J. Zhao, Phys. Rev. Lett. **116**, 107001 (2016).
- [20] L. Rademaker, Y. Wang, T. Berlijn, and S. Johnston, New J. Phys. **18**, 022001 (2016).
- [21] Y. Zhou and A. J. Millis, Phys. Rev. B **93**, 224506 (2016).
- [22] Z.-X. Li, F. Wang, H. Yao, and D. H. Lee, Science Bulletin **61**, 925 (2016).
- [23] Y. Wang, K. Nakatsukasa, L. Rademaker, T. Berlijn, and S. Johnston, Supercond. Sci. Technol. **29**, 054009 (2016).
- [24] M. L. Kulić and O. V. Dolgov, arXiv:1607.00843.
- [25] J. Shiogai, Y. Ito, T. Mitsuhashi, T. Nojima, and A. Tsukazaki, Nature Phys. **12**, 42 (2016).
- [26] Z. R. Ye, *et al.*, arXiv:1512.02526.
- [27] Y. Miyata, K. Nakayama, K. Sugawara, T. Sato, and T. Takahashi, Nature Mater. **14**, 775 (2015).
- [28] X. H. Niu, *et al.*, Phys. Rev. B **92**, 060504 (2015).
- [29] L. Zhao, *et al.*, Nat. Commun. **7**, 10608 (2016).
- [30] M. D. Watson, *et al.*, Phys. Rev. B **91**, 155106 (2015).
- [31] A. V. Chubukov, R. M. Fernandes, and J. Schmalian, Phys. Rev. B **91**, 201105 (2015).
- [32] A. V. Chubukov, M. Khodas, and R. M. Fernandes, arXiv:1602.05503.
- [33] F. Wang, S. A. Kivelson, and D.-H. Lee, Nature Phys. **11**, 959 (2015).
- [34] R. Yu and Q. Si, Phys. Rev. Lett. **115**, 116401 (2015).
- [35] J. K. Glasbrenner, I. I. Mazin, H. O. Jeschke, P. J. Hirschfeld, R. M. Fernandes, and R. Valenti, Nature Phys. **11**, 953 (2015).
- [36] Y. Zhang, *et al.*, Phys. Rev. B **94**, 115153 (2016).
- [37] C. H. P. Wen, *et al.*, Nat. Commun. **7**, 10840 (2016).
- [38] D. Huang, T. A. Webb, S. Fang, C.-L. Song, C.-Z. Chang, J. S. Moodera, E. Kaxiras, and J. E. Hoffman, Phys. Rev. B **93**, 125129 (2016).
- [39] H. Yamase and R. Zeyher, Phys. Rev. B **88**, 180502(R) (2013).
- [40] P. T. Dumitrescu, M. Serbyn, R. T. Scalettar, and A. Vishwanath, Phys. Rev. B **94**, 155127 (2016).
- [41] S. V. Borisenko, *et al.*, Nat. Phys. **12**, 311 (2016).
- [42] Q. Fan *et al.*, Nature Phys. **11**, 946 (2015).
- [43] R. Peng, *et al.*, Phys. Rev. Lett. **112**, 107001 (2014).
- [44] Z. Du, X. Yang, H. Lin, D. Fang, G. Du, J. Xing, H. Yang, X. Zhu, H.-H. Wen, Nat. Commun. **7**, 10565 (2016).
- [45] V. Cvetkovic and O. Vafek, Phys. Rev. B **88**, 134510 (2013).
- [46] R. M. Fernandes and O. Vafek, Phys. Rev. B **90**, 214514 (2014).
- [47] Y. Schattner, S. Lederer, S. A. Kivelson, and E. Berg, Phys. Rev. X **6**, 031028 (2016).
- [48] Z.-X. Li, F. Wang, H. Yao, and D. H. Lee, arXiv:1512.04541.
- [49] To be consistent with previous works, the irreducible representations refer to the actual crystallographic 2-Fe Brillouin zone coordinate system (K_x, K_y), i.e. B_{2g} transforms as $k_x^2 - k_y^2$ (or $K_x K_y$) and B_{1g} transforms as $k_x k_y$ (or $K_x^2 - K_y^2$).
- [50] A. Fedorov, *et al.*, arXiv:1606.03022.
- [51] R. M. Fernandes and A. J. Millis, Phys. Rev. Lett. **110**, 117004 (2013).
- [52] F. Yang, F. Wang, and D.-H. Lee, Phys. Rev. B **88**, 100504 (2013).
- [53] P. M. R. Brydon, S. Das Sarma, Hoi-Yin Hui, Jay D. Sau, Phys. Rev. B **90**, 184512 (2014).
- [54] Y. Wang, G. Y. Cho, T. L. Hughes, and E. Fradkin, Phys. Rev. B **93**, 134512 (2016).
- [55] S. Lederer, Y. Schattner, E. Berg, and S. A. Kivelson, Phys. Rev. Lett. **114**, 097001 (2015).
- [56] Y. Zhang, J. J. Lee, R. G. Moore, W. Li, M. Yi, M. Hashimoto, D. H. Lu, T. P. Devereaux, D.-H. Lee, and Z.-X. Shen, Phys. Rev. Lett. **117**, 117001 (2016).
- [57] N. Hao and J. Hu, Phys. Rev. X **4**, 031053 (2014).
- [58] M. Khodas and A. V. Chubukov, Phys. Rev. Lett. **108**, 247003 (2012).
- [59] A. Hinojosa and A. V. Chubukov, Phys. Rev. B **91**, 224502 (2015).
- [60] B. Li, Z. W. Xing, G. Q. Huang, and D. Y. Xing, J. Appl. Phys. **115**, 193907 (2014);

Supplementary Material for “Superconductivity in FeSe thin films driven by the interplay between nematic fluctuations and spin-orbit coupling”

I. SUPERCONDUCTING GAP EQUATIONS

A. No spin-orbit coupling

The non-interacting Hamiltonian in terms of the spinors $\psi_{X,Y}$ is given by $\mathcal{H}_0 = \sum_{\mathbf{k}, i=X,Y} \Psi_i^\dagger(\mathbf{k}) \hat{H}_i(\mathbf{k}) \Psi_i(\mathbf{k})$, with:

$$\hat{H}_X = \begin{pmatrix} \epsilon_1 + \frac{\mathbf{K}^2}{2m_1} - a_1 K_x K_y & -iv_-(\mathbf{K}) \\ iv_-(\mathbf{K}) & \epsilon_3 + \frac{\mathbf{K}^2}{2m_3} - a_3 K_x K_y \end{pmatrix}, \quad \hat{H}_Y = \begin{pmatrix} \epsilon_1 + \frac{\mathbf{K}^2}{2m_1} + a_1 K_x K_y & -iv_+(\mathbf{K}) \\ iv_+(\mathbf{K}) & \epsilon_3 + \frac{\mathbf{K}^2}{2m_3} + a_3 K_x K_y \end{pmatrix} \quad (\text{S1})$$

and

$$v_{\pm}(\mathbf{K}) = v(\pm K_x + K_y) + p_1(\pm K_x^3 + K_y^3) + p_2 K_x K_y (K_x \pm K_y). \quad (\text{S2})$$

where (K_x, K_y) refer to the 2-Fe Brillouin zone (BZ). The parameters in the Hamiltonian \mathcal{H}_0 are taken from Table IX of Ref. [S1]. The SC gap equations are given by the Feynman diagram in Fig. S1:

$$\eta_\alpha \hat{M}_\alpha = \chi_{\text{nem}} T \sum_{n, \mathbf{k}} \left(\hat{\lambda}^{\text{nem}} \right)^T \hat{G}_{-k}^T \hat{M}_\alpha \hat{G}_k \hat{\lambda}^{\text{nem}}. \quad (\text{S3})$$

where $\hat{\lambda}$, \hat{G}_K are 4×4 matrices:

$$\hat{\lambda}^{\text{nem}} = \begin{pmatrix} \hat{\lambda}_X^{\text{nem}} & 0 \\ 0 & \hat{\lambda}_Y^{\text{nem}} \end{pmatrix}, \quad \hat{G}_K = (i\omega_n I_{4 \times 4} - H(\mathbf{K}))^{-1} \text{ with } \hat{H}(\mathbf{K}) = \begin{pmatrix} \hat{H}_X(\mathbf{K}) & 0 \\ 0 & \hat{H}_Y(\mathbf{K}) \end{pmatrix}$$

and $\hat{\lambda}_X^{\text{nem}}$ and $\hat{\lambda}_Y^{\text{nem}}$ are defined as in the main text. For simplicity, we introduce two parameters to describe the nematic couplings λ_1 and λ_2 : $\lambda = \sqrt{\lambda_1^2 + \lambda_2^2}$ and $\chi = \tan^{-1}(\lambda_2/\lambda_1)$. \hat{M}_α is also a 4×4 matrix with the label α referring to different irreducible representations of the $P4/nmm$ space group. Following Ref. [S1], there are 6 different irreducible representations corresponding to singlet pairing at the electron pockets (namely, A_{1g} , B_{2g} , A_{2u} , B_{2u} , E_g , and E_u):

$$\begin{aligned} \hat{M}_{A_{1g}/B_{2g}} &= \begin{pmatrix} \Delta_1 & & \\ & \Delta_2 & \\ & & \pm \Delta_1 \\ & & & \pm \Delta_2 \end{pmatrix} & \hat{M}_{A_{2u}/B_{2u}} &= \begin{pmatrix} 0 & \frac{\tau_0 \pm \tau_3}{2} \\ \frac{\tau_0 \pm \tau_3}{2} & 0 \end{pmatrix} & \hat{M}_{E_g^{(1)}} &= \begin{pmatrix} 0 & \tau_- \\ \tau_+ & 0 \end{pmatrix} \\ \hat{M}_{E_g^{(2)}} &= \begin{pmatrix} 0 & -\tau_+ \\ -\tau_- & 0 \end{pmatrix} & \hat{M}_{E_u^{(1)}} &= \begin{pmatrix} 0 & 0 \\ 0 & \tau_1 \end{pmatrix} & \hat{M}_{E_u^{(2)}} &= \begin{pmatrix} \tau_1 & 0 \\ 0 & 0 \end{pmatrix} \end{aligned} \quad (\text{S4})$$

Note that because E_g and E_u are two-dimensional representations, we introduced the superscripts (1) and (2) for the two components of the representation that give the same eigenvalue η . To compute T_c , we note that an infinitesimal pairing field Δ_0 is renormalized by nematic fluctuations according to the diagrammatic series shown in Fig. S1:

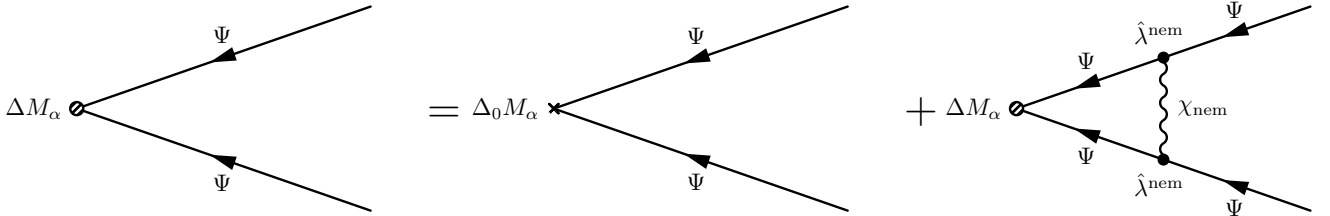


FIG. S1: The effective pairing field ΔM_α is the sum of the infinitesimal pairing field $\Delta_0 M_\alpha$ and the effective pairing field dressed by nematic fluctuations.

$$\Delta \hat{M}_\alpha = \Delta_0 \hat{M}_\alpha + \Delta \chi_{\text{nem}} T \sum_{n,\mathbf{k}} \left(\hat{\lambda}^{\text{nem}} \right)^T \hat{G}_{-k}^T \hat{M}_\alpha \hat{G}_k \hat{\lambda}^{\text{nem}} \implies \Delta = \frac{\Delta_0}{1 - \eta_\alpha} \quad (\text{S5})$$

Therefore, T_c is obtained when the largest eigenvalue $\eta_\alpha(T = T_c) = 1$. In our paper, the value of the coupling $\lambda^2 \chi_{\text{nem}}$ is set such that $T_c = 5$ meV for the case of A_{1g}/B_{2g} pairing when $\lambda_2 = 0$, i.e. $\chi = 0$. Fig. S2 shows the other eigenvalues η_α at the same temperature $T = 5$ meV. Clearly, the A_{1g} and B_{1g} states are the degenerate leading SC instabilities of this system. The corresponding values for Δ_1 and Δ_2 as a function of $\chi = \tan^{-1}(\lambda_2/\lambda_1)$ is also shown in the figure.

To project the gaps onto the Fermi pockets, $\Delta_{X/Y}(\mathbf{K})$, we introduce the spinor $u_{X/Y}(\mathbf{K}) = (u_{X/Y,1}(\mathbf{K}), u_{X/Y,2}(\mathbf{K}))^T$ that diagonalizes $\hat{H}_{X/Y}$ and whose eigenvalue corresponds to the band dispersion that crosses the Fermi level. Then, the projected gap is given by:

$$\Delta_X(\mathbf{K}) = \Delta_1 |u_{X,1}(\mathbf{K})|^2 + \Delta_2 |u_{X,2}(\mathbf{K})|^2 \quad (\text{S6})$$

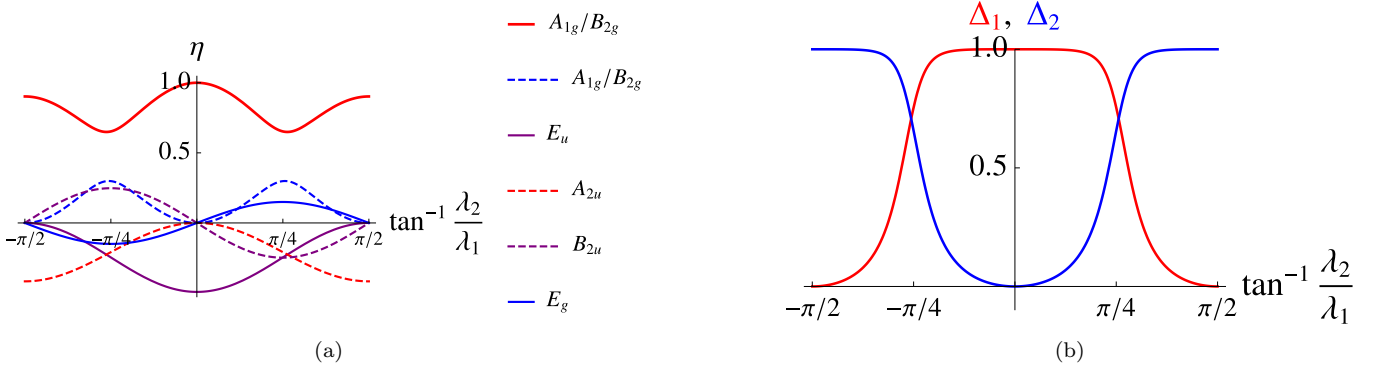


FIG. S2: (a) The eigenvalues for different SC channels without SOC or ISB, as function of the ratio λ_2/λ_1 between the two nematic coupling constants. (b) The two intra-orbital gap functions Δ_1 and Δ_2 corresponding to the solution of the gap equations in the degenerate A_{1g}/B_{2g} channel.

B. Non-zero spin-orbit coupling

The SOC interaction is given by:

$$\mathcal{H}_{\text{SOC}} = \frac{i}{2} \lambda_{\text{SOC}} \Psi_Y^\dagger (\tau_+ \otimes \sigma_1 + \tau_- \otimes \sigma_2) \Psi_X + h.c. \quad (\text{S7})$$

In the presence of SOC, spin-singlet and spin-triplet pairings are mixed. In general, the latter can be written as $\Psi^T \mathbf{M} \otimes i\sigma_2 \boldsymbol{\sigma} \Psi$, where Ψ is the eight-component spinor $\Psi = (\Psi_{X\sigma}, \Psi_{Y\sigma})^T$. Since the spin component is symmetric for spin-triplet pairing, the orbital part \mathbf{M} must be anti-symmetric. Since A_{1g} and B_{2g} are the two leading SC instabilities in the absence of SOC, we only focus on these two channels here. These irreducible representations can only be obtained if both the spin component and the orbital component transform as E_g , since $E_g \otimes E_g = A_{1g} \oplus A_{2g} \oplus B_{1g} \oplus B_{2g}$. The spin combination that transforms according to E_g is $(i\sigma_2\sigma_1, i\sigma_2\sigma_2)$; for the orbital part, which must be anti-symmetric (i.e. E_g^-), we have:

$$-i(\Psi_Y^T \tau_+ \Psi_X - \Psi_X^T \tau_- \Psi_Y, \Psi_Y^T \tau_- \Psi_X - \Psi_X^T \tau_+ \Psi_Y) \quad (\text{S8})$$

which corresponds to inter-pocket pairing. Writing it in the form $(\Psi^T M_1 \Psi, \Psi^T M_2 \Psi)$, we readily obtain the non-zero matrix elements $(M_2)_{14} = -(M_2)_{41} = (M_1)_{23} = -(M_1)_{32} = i$. Combined with the spin part, we obtain the following

gap functions:

$$A_{1g} : \quad \Psi^T \left(\begin{pmatrix} \Delta_1^A & 0 & 0 & 0 \\ 0 & \Delta_2^A & 0 & 0 \\ 0 & 0 & \Delta_1^A & 0 \\ 0 & 0 & 0 & \Delta_2^A \end{pmatrix} \otimes i\sigma_2 + \begin{pmatrix} 0 & 0 & 0 & 0 \\ 0 & 0 & i\Delta_3^A & 0 \\ 0 & -i\Delta_3^A & 0 & 0 \\ 0 & 0 & 0 & 0 \end{pmatrix} \otimes \sigma_3 + \begin{pmatrix} 0 & 0 & 0 & -\Delta_3^A \\ 0 & 0 & 0 & 0 \\ 0 & 0 & 0 & 0 \\ \Delta_3^A & 0 & 0 & 0 \end{pmatrix} \otimes \sigma_0 \right) \Psi \quad (S9)$$

$$B_{2g} : \quad \Psi^T \left(\begin{pmatrix} \Delta_1^B & 0 & 0 & 0 \\ 0 & \Delta_2^B & 0 & 0 \\ 0 & 0 & -\Delta_1^B & 0 \\ 0 & 0 & 0 & -\Delta_2^B \end{pmatrix} \otimes i\sigma_2 + \begin{pmatrix} 0 & 0 & 0 & 0 \\ 0 & 0 & i\Delta_3^B & 0 \\ 0 & -i\Delta_3^B & 0 & 0 \\ 0 & 0 & 0 & 0 \end{pmatrix} \otimes \sigma_3 + \begin{pmatrix} 0 & 0 & 0 & \Delta_3^B \\ 0 & 0 & 0 & 0 \\ 0 & 0 & 0 & 0 \\ -\Delta_3^B & 0 & 0 & 0 \end{pmatrix} \otimes \sigma_0 \right) \Psi \quad (S10)$$

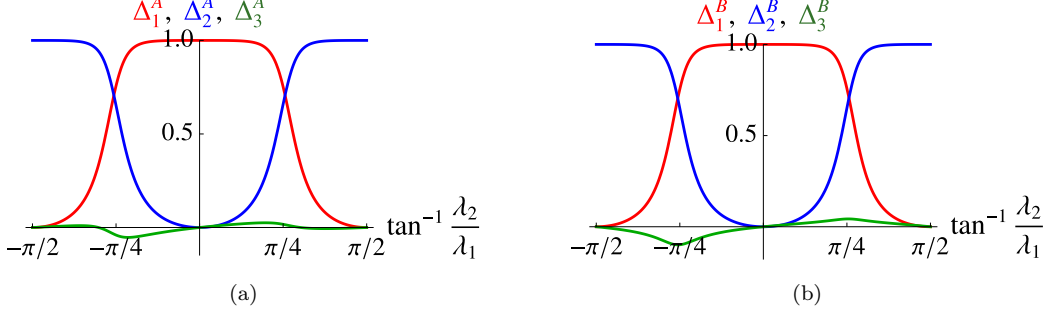


FIG. S3: The solution of the A_{1g} and B_{2g} pairing gaps in the presence of SOC. The two nematic couplings are given by λ_1 and λ_2 .

The three gaps Δ_1 , Δ_2 , and Δ_3 are determined by solving the gap equation. In Fig. S3, we show the solution of the gap equations: clearly, the presence of spin-orbit coupling lifts the degeneracy between A_{1g} and B_{2g} , as illustrated in Fig. 2 of the main text. Here we used $\lambda_{\text{SOC}} = 50\text{meV}$. We also note that the admixture with the triplet component is small.

To calculate the momentum dependence of the gap function, we project the gaps Δ_1 , Δ_2 , and Δ_3 along the Fermi surface. Since the Hamiltonian does not break time reversal symmetry and inversion symmetry, each band is doubly degenerate (Kramers degeneracy). To show this more clearly, we define two new 4-component spinors related by time reversal symmetry:

$$\Phi_1 = (\Psi_{X\uparrow} \quad \Psi_{Y\downarrow}) , \quad \text{and} \quad \Phi_2 = (\Psi_{X\downarrow} \quad -\Psi_{Y\uparrow}) \quad (S11)$$

Both \mathcal{H}_0 and the SOC term are diagonal in this representation:

$$\mathcal{H}_0 + \mathcal{H}_{\text{SOC}} = \sum_{\mathbf{K}} \Phi_1^\dagger \hat{H}_1 \Phi_1 + \sum_{\mathbf{K}} \Phi_2^\dagger \hat{H}_2 \Phi_2 , \quad \text{with} \quad \hat{H}_1 = \begin{pmatrix} \hat{H}_X & \hat{h} \\ \hat{h}^\dagger & \hat{H}_Y \end{pmatrix} , \quad \hat{H}_2 = \begin{pmatrix} \hat{H}_X & \hat{h}^* \\ \hat{h}^T & \hat{H}_Y \end{pmatrix} , \quad \text{and} \quad \hat{h} = \frac{\lambda_{\text{SOC}}}{2} \begin{pmatrix} 0 & -1 \\ -i & 0 \end{pmatrix}$$

It follows immediately that $H_1(\mathbf{K}) = H_2^*(-\mathbf{K})$. Furthermore, because the system is also invariant under inversion, the energy dispersions of Φ_1 and Φ_2 are exactly the same. This implies that each band in the system is doubly degenerate, although neither Φ_1 nor Φ_2 has degeneracies. Upon diagonalization, we find that the two overlapping electron pockets split due to the SOC, forming an inner and an outer electron pocket.

As for the pairing interaction, we find that both A_{1g} and B_{2g} gaps couple the two spinors, $\Phi_1^T \hat{\Delta}_{A_{1g}} \Phi_2$ and $\Phi_1^T \hat{\Delta}_{B_{2g}} \Phi_2$, with

$$\hat{\Delta}_{A_{1g}} = \begin{pmatrix} \Delta_1^A & 0 & 0 & \Delta_3^A \\ 0 & \Delta_2^A & -i\Delta_3^A & 0 \\ 0 & i\Delta_3^A & \Delta_1^A & 0 \\ \Delta_3^A & 0 & 0 & \Delta_2^A \end{pmatrix} , \quad \text{and} \quad \hat{\Delta}_{B_{2g}} = \begin{pmatrix} \Delta_1^B & 0 & 0 & -\Delta_3^B \\ 0 & \Delta_2^B & -i\Delta_3^B & 0 \\ 0 & i\Delta_3^B & -\Delta_1^B & 0 \\ -\Delta_3^B & 0 & 0 & -\Delta_2^B \end{pmatrix}$$

This allows us to project the gap onto the Fermi surface in a straightforward way. Consider for instance the A_{1g} gap projected onto the inner Fermi pocket. We first diagonalize $H_1(\mathbf{K})$ and $H_2(\mathbf{K})$ to obtain the band operators

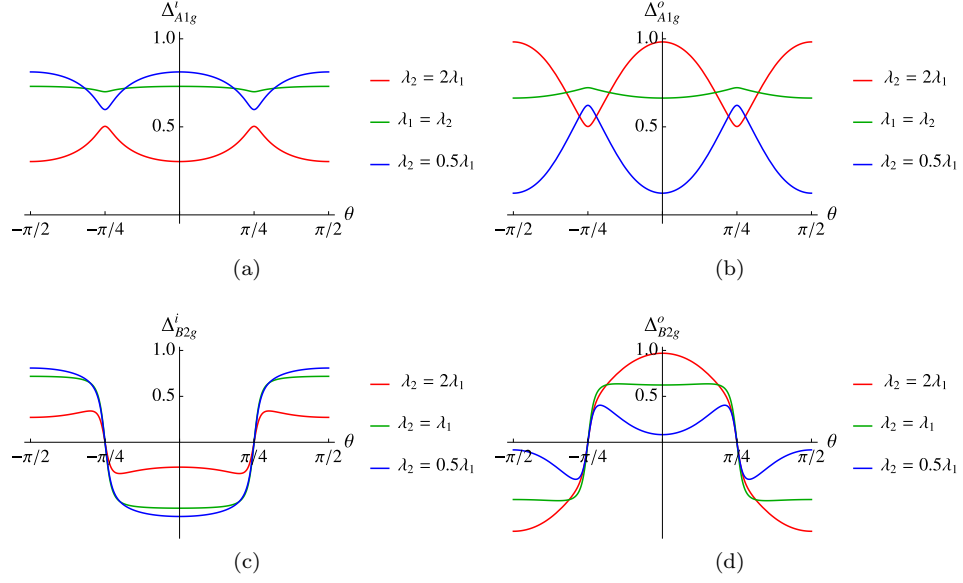


FIG. S4: Projected gap on the inner (*i*) and outer (*o*) electron pockets, with $\lambda_{\text{SOC}} = 50\text{meV}$. (a) and (b) correspond to the A_{1g} pairing channel, whereas (c) and (d) correspond to the B_{2g} channel. The two nematic couplings are given by λ_1 and λ_2 .

$u_{i,\mathbf{K}}$ and $v_{i,\mathbf{K}}$, respectively. They are related to the orbital operators $d_{\mu,\mathbf{K}}$ according to:

$$d_{\mu,\mathbf{K}} = \sum_i \langle \mu | u_i(\mathbf{K}) \rangle u_{i,\mathbf{K}} \quad (\text{S12})$$

$$d_{\mu,\mathbf{K}} = \sum_i \langle \mu | v_i(\mathbf{K}) \rangle v_{i,\mathbf{K}} \quad (\text{S13})$$

Due to time-reversal symmetry, $\langle \mu | v_i(-\mathbf{K}) \rangle = \langle u_i(\mathbf{K}) | d_\mu \rangle$. The SC Hamiltonian then becomes:

$$\begin{aligned} \sum_{\mu\nu} \Delta_{\mu\nu} d_{\mu,-\mathbf{K}} d_{\nu,\mathbf{K}} &= \sum_{\mu\nu} \Delta_{\mu\nu} \sum_{ij} \langle \mu | v_i(-\mathbf{K}) \rangle \langle \nu | u_j(\mathbf{K}) \rangle v_{i,-\mathbf{K}} u_{j,\mathbf{K}} \\ &= \sum_{\mu\nu} \Delta_{\mu\nu} \sum_{ij} \langle u_i(\mathbf{K}) | \mu \rangle \langle \nu | u_j(\mathbf{K}) \rangle v_{i,-\mathbf{K}} u_{j,\mathbf{K}} \end{aligned} \quad (\text{S14})$$

Projecting onto band l , we find:

$$\sum_{\mu\nu} \Delta_{\mu\nu} \langle u_l(\mathbf{K}) | \mu \rangle \langle \nu | u_l(\mathbf{K}) \rangle v_l(-\mathbf{K}) u_l(\mathbf{K}) = \langle u_l(\mathbf{K}) | \hat{\Delta} | u_l(\mathbf{K}) \rangle v_l(-\mathbf{K}) u_l(\mathbf{K}) \quad (\text{S15})$$

As a result, the gap along the pocket corresponding to band l given by:

$$\Delta_l(\mathbf{K}) = \langle u_l(\mathbf{K}) | \hat{\Delta} | u_l(\mathbf{K}) \rangle, \quad (\text{S16})$$

yielding the results shown in Fig. S4.

C. Inversion symmetry-breaking

As discussed in the main text, the inversion symmetry is broken at the interface of thin films of FeSe. Considering the generators of the $P4/nmm$ group, $\{\sigma_z | \frac{1}{2} \frac{1}{2}\}$ is the only symmetry transformation broken, as it corresponds to a reflection σ_z with respect to the Fe plane followed by a translation by $(\frac{1}{2}, \frac{1}{2})$ in the 2-Fe unit cell. Because the term:

$$H_{\text{ISB}} = \lambda_{\text{ISB}} \Psi_X^\dagger \frac{\tau_0 + \tau_3}{2} \Psi_Y + h.c. \quad (\text{S17})$$

acquires a minus sign upon the symmetry transformation $\{\sigma_z|\frac{1}{2}\frac{1}{2}\}$, it must be generated once inversion symmetry is broken. Similarly to the SOC term, the ISB term hybridizes the X and Y pockets, and splits the degeneracy between the A_{1g} and B_{2g} pairing states. Unlike the SOC case, there is no admixture with triplet components. However, to solve the gap equations, one needs to introduce an admixture with the pairing channel A_{2u} , resulting in the pairing matrix of the form:

$$\hat{M}_{A_{1g}+A_{2u}} = \begin{pmatrix} \Delta_1 & 0 & \Delta_3 & 0 \\ 0 & \Delta_2 & 0 & 0 \\ \Delta_3 & 0 & \Delta_1 & 0 \\ 0 & 0 & 0 & \Delta_2 \end{pmatrix} \quad (\text{S18})$$

In Fig. S5, we show the solution of the gap equations and the corresponding gap functions projected onto the Fermi surface.

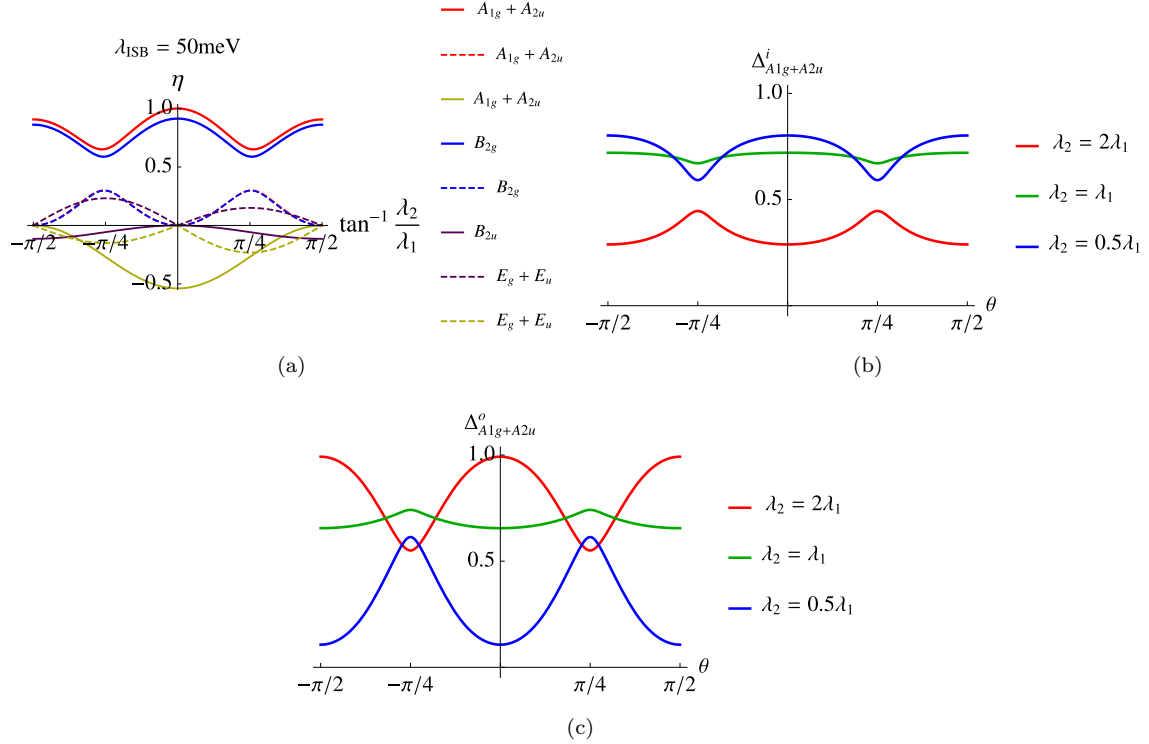


FIG. S5: (a) The SC eigenvalue η in different SC channels for $\lambda_{\text{ISB}} = 50 \text{ meV}$. (b) and (c): Projected gap on the inner (i) and outer (o) electron pockets in the leading $A_{1g} + A_{2u}$ pairing channel. The two nematic couplings are given by λ_1 and λ_2 .

II. SUPERCONDUCTING FREE ENERGY

A. No spin-orbit coupling

In the absence of SOC and ISB, the s -wave and d -wave channels have the same T_c . In terms of a free energy expansion, this implies that, to quadratic order in the gaps:

$$F^{(2)} = \alpha (|\Delta_s|^2 + |\Delta_d|^2) \quad (\text{S19})$$

In this section we study how this degeneracy is affected by quartic coefficients in the free energy, which go beyond the linearized SC gap equations. For notation convenience, we define the superconducting order parameters Δ_s and

Δ_d by

$$\hat{\Delta}_{A_{1g}} = \Delta_s \begin{pmatrix} \cos \alpha_s & 0 & 0 & 0 \\ 0 & \sin \alpha_s & 0 & 0 \\ 0 & 0 & \cos \alpha_s & 0 \\ 0 & 0 & 0 & \sin \alpha_s \end{pmatrix} \otimes i\sigma_2 \quad \hat{\Delta}_{B_{2g}} = \Delta_d \begin{pmatrix} \cos \alpha_d & 0 & 0 & 0 \\ 0 & \sin \alpha_d & 0 & 0 \\ 0 & 0 & -\cos \alpha_d & 0 \\ 0 & 0 & 0 & -\sin \alpha_d \end{pmatrix} \otimes i\sigma_2 .$$

They are related to the gaps $\Delta_{1,2}^{A/B}$ according to $\Delta_1^{A/B} = \Delta_{s/d} \cos \alpha_{s/d}$ and $\Delta_2^{A/B} = \Delta_{s/d} \sin \alpha_{s/d}$. The parameters $\alpha_{s/d}$ are obtained from the gap equations. The quartic terms of the free energy are given by:

$$F^{(4)} = \frac{T}{2} \sum_k \text{Tr} \left(\hat{G}_k \hat{\Delta} \hat{G}_{-k}^T \hat{\Delta}^\dagger \hat{G}_k \hat{\Delta} \hat{G}_{-k}^T \hat{\Delta}^\dagger \right), \quad \text{with} \quad \hat{\Delta} = \hat{\Delta}_{A_{1g}} + \hat{\Delta}_{B_{2g}} .$$

yielding:

$$F^{(4)} = \beta_1 |\Delta_d|^4 + \gamma_1 |\Delta_s|^2 |\Delta_d|^2 + \frac{\gamma_2}{2} (\Delta_s^{*2} \Delta_d^2 + c.c.) + \beta_2 |\Delta_d|^4, \quad (\text{S20})$$

Evaluating the trace gives $\gamma_1 = 2\gamma_2 = 4\beta_1 = 4\beta_2 = 4\beta$. Thus, the free energy can be written as

$$F = \alpha (|\Delta_s|^2 + |\Delta_d|^2) + \beta (|\Delta_s|^4 + |\Delta_d|^4 + 4|\Delta_s|^2 |\Delta_d|^2 + \Delta_s \Delta_d^* + \Delta_s^* \Delta_d) \quad (\text{S21})$$

Minimizing the free energy with respect to the relative phase between Δ_s and Δ_d give $\pi/2$. Under this condition, the free energy is given by:

$$F = \alpha (|\Delta_s|^2 + |\Delta_d|^2) + \beta (|\Delta_s|^2 + |\Delta_d|^2)^2 \quad (\text{S22})$$

Thus, besides the $U(1)$ symmetry related to the global phase, there is an additional $U(1)$ symmetry related to the fact that only the value of $|\Delta_s|^2 + |\Delta_d|^2$ is fixed by minimization of the free energy. Equivalently, we can write the s and d gaps in terms of the gaps on the two electron pockets, Δ_X and Δ_Y . To see this, we note that the solution of the gap equations for the s and d gaps give the same parameter $\alpha_s = \alpha_d$. Then the total gap can be written as:

$$\hat{\Delta} = \hat{\Delta}_{A_{1g}} + \hat{\Delta}_{B_{2g}} = \begin{pmatrix} (\Delta_s + \Delta_d) \tilde{\tau} & 0 \\ 0 & (\Delta_s - \Delta_d) \tilde{\tau} \end{pmatrix} \quad (\text{S23})$$

with the 2×2 diagonal matrix $\tilde{\tau} = \text{diag}(\cos \alpha_s, \sin \alpha_s)$. Since the upper (lower) diagonal block is related to the X (Y) pocket, we have:

$$\Delta_X = \Delta_s + \Delta_d, \quad \Delta_Y = \Delta_s - \Delta_d$$

Substitution in the free energy yields two decoupled superconducting systems:

$$F = \frac{\alpha}{2} (|\Delta_X|^2 + |\Delta_Y|^2) + \frac{\beta}{2} (|\Delta_X|^4 + |\Delta_Y|^4) \quad (\text{S24})$$

B. Non-zero spin-orbit coupling and inversion symmetry-breaking

The main effect of the SOC (and also of the ISB) is to generate a quadratic coupling between the two gaps Δ_X and Δ_Y . According to the Feynman diagram of Fig. 3 in the main text, these terms generate the quadratic contribution to the free energy:

$$\delta F = \gamma (\Delta_X \Delta_Y^* + \Delta_X^* \Delta_Y) \quad (\text{S25})$$

Here we illustrate the computation of γ for the case of SOC. The Feynman diagram gives:

$$\begin{aligned} \gamma &= - \left(\frac{i\lambda}{2} \right)^2 T \sum_{n, \mathbf{k}} \text{Tr} \left[\Delta_X \otimes i\sigma_2 G_X(\omega_n, \mathbf{K}) (\tau_+ \otimes \sigma_1 + \tau_- \otimes \sigma_2) G_Y(\omega_n, \mathbf{K}) \Delta_Y^* \otimes (-i\sigma_2) G_Y^T(-\omega_n, -\mathbf{K}) \right. \\ &\quad \left. (\tau_+ \otimes \sigma_1 + \tau_- \otimes \sigma_2)^T G_X^T(-\omega_n, -\mathbf{K}) \right] \\ &= - \frac{\lambda^2}{2} T \sum_{n, \mathbf{k}} \{ (G_Y \Delta_Y^* G_Y^T)_{22} (G_X^T \Delta_X G_X)_{11} + (G_Y \Delta_Y^* G_Y^T)_{11} (G_X^T \Delta_X G_X)_{22} \} \end{aligned} \quad (\text{S26})$$

where $G_{X/Y} = (i\omega_n - H_{X/Y}(K))^{-1}$ and $G_{X/Y}^T = (-i\omega_n - H_{X/Y}^T(-\mathbf{K}))^{-1}$. In general, the diagonal component of $G_X^T \Delta_X G_X$ could be either positive or negative. But if we only focus on the projection along the band that crosses the Fermi level, this diagonal component must be positive. Consider for instance the wave-function $|u(\mathbf{K})\rangle$ that diagonalizes $H_X(\mathbf{K})$ and gives the band $\epsilon_u(\mathbf{K})$ that crosses the Fermi surface. We find:

$$(G_X^T \Delta_X G_X)_{ii} \approx \frac{\langle u(\mathbf{K}) | \Delta_X | u(\mathbf{K}) \rangle |\langle i | u(\mathbf{K}) \rangle|^2}{(-i\omega_n - \epsilon_u(\mathbf{K}))(i\omega_n - \epsilon_u(\mathbf{K}))} = \frac{|\langle i | u(\mathbf{K}) \rangle|^2}{\omega_n^2 + \epsilon_u^2(\mathbf{K})} \langle u(\mathbf{K}) | \Delta_X | u(\mathbf{K}) \rangle \quad (\text{S27})$$

Since:

$$\langle u(\mathbf{k}) | \Delta_X | u(\mathbf{k}) \rangle = \Delta_1 |u_1(\mathbf{k})|^2 + \Delta_2 |u_2(\mathbf{k})|^2$$

is the SC gap projected onto the band that crosses the Fermi level, we find that it is always positive, because both Δ_1 and Δ_2 are positive, as shown in Fig. S2. Thus, it follows that $\gamma < 0$.

As for the quartic coefficients, we find that in the presence of SOC or ISB they satisfy the relationship $\gamma_1 - \gamma_2 \lesssim 2\sqrt{\beta_1 \beta_2}$. As a result, the two gap functions can in principle coexist and break time reversal symmetry at low temperatures.

C. Large-momentum nematic fluctuations

In the previous subsection, we investigated the effect of SOC and ISB in lifting the *s*-wave/*d*-wave degeneracy. It is interesting to study whether large-momentum nematic fluctuations, involving momentum transfer $\mathbf{q} \approx \mathbf{M} = (\pi, \pi)$ and thus coupling the electron pockets, give rise to a similar effect. We note that these large-momentum fluctuations are actually associated with orbital order that breaks translational symmetry (antiferro-orbital order), instead of ferro-orbital order. The fact that the associated antiferro-orbital order has not been observed in bulk or thin films of FeSe suggests that these fluctuations are much smaller than the nematic ones, and therefore can be considered a perturbation on top of the superconducting state obtained previously. For this reason, the main contribution of the large-momentum nematic fluctuations χ_M to the superconducting free energy is captured by the Feynman diagram in Fig. S6, yielding the quadratic term:

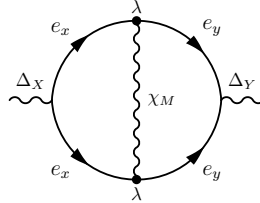


FIG. S6: Feynman diagram representing the coupling between the gaps in the two electron pockets mediated by large-momentum nematic fluctuations $\chi_{nem}(\mathbf{q} \approx \mathbf{M}) \equiv \chi_M$. Similar to SOC, this coupling also lifts the degeneracy between *s*-wave and *d*-wave, but with a much smaller effect.

$$\delta F = \gamma' (\Delta_X^* \Delta_Y + \Delta_Y^* \Delta_X) \quad (\text{S28})$$

with

$$\begin{aligned} \gamma' &= -T^2 \sum_{m,n} \int \frac{d^2 \mathbf{k}}{(2\pi)^2} \frac{d^2 \mathbf{k}'}{(2\pi)^2} \frac{\lambda^2 \chi(\omega_n - \omega_m, \mathbf{k} - \mathbf{k}' + \mathbf{M})}{(i\omega_n - \epsilon_X(\mathbf{k}))(-i\omega_n - \epsilon_X(-\mathbf{k}))(i\omega_m - \epsilon_Y(\mathbf{k}'))(-i\omega_m - \epsilon_Y(-\mathbf{k}'))} \\ &\approx -\lambda^2 \chi_M T^2 \sum_{m,n} \int \frac{d^2 \mathbf{k}}{(2\pi)^2} \frac{d^2 \mathbf{k}'}{(2\pi)^2} \frac{1}{(\omega_n^2 + \epsilon_X^2(\mathbf{k}))(\omega_m^2 + \epsilon_Y^2(\mathbf{k}'))} \\ &\approx -N_f^2 \lambda^2 \chi_M \left(\ln \frac{\Lambda}{T_c} \right)^2 \end{aligned} \quad (\text{S29})$$

In the above formula, we made the approximation that the nematic susceptibility is peaked at zero frequency and momentum \mathbf{Q} , and neglected the orbital dependence of the coupling between the fermions and the nematic fluctuation. It is obvious that $\gamma' < 0$, showing that the nematic fluctuation χ_M also favors s wave.

Next, we compare the effects of large-momentum fluctuations and SOC in lifting the degeneracy by comparing γ' calculated here with γ calculated in Eq. (S25). From Fig. 3, we can estimate γ as:

$$\gamma \approx -T \sum_n \int \frac{d^2 \mathbf{k}}{(2\pi)^2} \frac{\lambda_{SOC}^2}{(\omega_n^2 + \epsilon_x^2(\mathbf{k}))(\omega_n^2 + \epsilon_y^2(\mathbf{k}))} \approx -\lambda_{SOC}^2 T \sum_n \int \frac{d^2 \mathbf{k}}{(2\pi)^2} \frac{1}{(\omega_n^2 + \epsilon^2(\mathbf{k}))^2} \sim -N_f \frac{\lambda_{SOC}^2}{T_c^2}$$

Furthermore, we can use for T_c :

$$\ln \frac{\Lambda}{T_c} \approx \frac{1}{N_f \lambda^2 \chi_0} \quad (\text{S30})$$

where χ_0 is the zero-momentum nematic susceptibility. Substituting in the equations above, we find:

$$\frac{\gamma}{\gamma'} = \frac{\chi_0}{\chi_M} \frac{\lambda_{SOC}^2}{T_c^2} \left(\ln \frac{\Lambda}{T_c} \right)^{-1} \approx (1 + 2\pi^2 \xi_{\text{nem}}^2 a^{-2}) \frac{\lambda_{SOC}^2}{T_c^2} \left(\ln \frac{\Lambda}{T_c} \right)^{-1} \quad (\text{S31})$$

where, in the last step, we considered the expansion $\chi_{\text{nem}}^{-1}(\mathbf{q}) = \xi_{\text{nem}}^{-2} + q^2$ and substituted $\chi_0 = \chi_{\text{nem}}(0)$, $\chi_0 = \chi_{\text{nem}}(\pi, \pi)$. We now substitute reasonable, experimentally-based values for these quantities. According to ARPES data in bulk FeSe [S3], $\lambda_{SOC} \approx 10$ meV, which is of the same order as $T_c \approx 6$ meV of the thin films. The bandwidth can be estimated as $\Lambda \sim 100$ meV, whereas the nematic correlation length is certainly a few lattice constants – say $\xi = 5a$. Substituting these numbers, we estimate $\gamma/\gamma' \approx 500 \gg 1$. Therefore, the effect of large-momentum fluctuations is negligible compared to the effect of spin-orbit coupling. A similar analysis for the inversion symmetry-breaking contribution reveals the latter is also much larger than the large-momentum fluctuations contribution, as long as $\lambda_{ISB} > 1$ meV. Although this is a reasonable value, first principle calculations are necessary to estimate λ_{ISB} , which is beyond the scope of this paper.

III. FERMI-SURFACE PROJECTED MODEL

In the previous analyses, we considered the low-energy model derived directly from the 5×5 tight-binding Hamiltonian. To gain more insight into the problem, we can further restrict our analysis only to the bands that cross the Fermi level, since they give the dominant contribution to the pairing instability. It is then convenient to write the X and Y pockets dispersions (here \mathbf{k} refers to the 1-Fe unit cell):

$$\varepsilon_{X,\mathbf{k}} = \frac{k^2}{2m} - \epsilon_\mu - \epsilon_m \cos 2\theta, \quad \varepsilon_{Y,\mathbf{k}} = \frac{k^2}{2m} - \epsilon_\mu + \epsilon_m \cos 2\theta \quad (\text{S32})$$

and the non-interacting Hamiltonian in terms of the band operators f_X and f_Y :

$$H_0 = \sum_{\mathbf{k}} \varepsilon_{X,\mathbf{k}} f_{X,\mathbf{k}}^\dagger f_{X,\mathbf{k}} + \sum_{\mathbf{k}} \varepsilon_{Y,\mathbf{k}} f_{Y,\mathbf{k}}^\dagger f_{Y,\mathbf{k}} \quad (\text{S33})$$

Here, ϵ_m gives the mismatch between the two electron pockets. The advantage of this model over the previous one is that it allows us to easily tune the ratio between the mismatch and the SOC, ϵ_m/λ_{SOC} , which in the full model above is fixed by the parameter v in Eq. S1. To proceed, we write down the relationship between the band operators f_X , f'_X and the orbital operators d_{xy} , d_{yz} [S2]:

$$f_X(\theta) = \frac{\alpha d_{xy} + i \sin \theta d_{yz}}{\sqrt{\alpha^2 + \sin^2 \theta}}; \quad f'_X(\theta) = \frac{i \sin \theta d_{xy} + \alpha d_{yz}}{\sqrt{\alpha^2 + \sin^2 \theta}}. \quad (\text{S34})$$

where θ is the polar angle. The factor i is inserted to keep the wave-function time-reversal invariant. While f_X describes the band obtained from the diagonalization of \hat{H}_X that crosses the Fermi level, f'_X describes the band that do not cross the Fermi level. These relationships can be inverted to give:

$$d_{xy} = \frac{\alpha f_X - i \sin \theta f'_X}{\sqrt{\alpha^2 + \sin^2 \theta}}, \quad d_{yz} = \frac{-i \sin \theta f_X + \alpha f'_X}{\sqrt{\alpha^2 + \sin^2 \theta}}. \quad (\text{S35})$$

The band operators f_Y, f'_Y , related to the Y pocket, are obtained by a rotation of $\pi/2$ followed by a mirror reflection σ_z with respect to the (x, y) plane:

$$\theta \rightarrow \theta - \frac{\pi}{2}, \quad d_{xy} \rightarrow -d_{xy}, \quad d_{yz} \rightarrow d_{xz} \quad \Rightarrow \quad f_Y(\theta) = -\frac{\alpha d_{xy} + i \cos \theta d_{xz}}{\sqrt{\alpha^2 + \cos^2 \theta}}; \quad f'_Y(\theta) = \frac{i \cos \theta d_{xy} + \alpha d_{xz}}{\sqrt{\alpha^2 + \cos^2 \theta}}.$$

The coupling between nematic fluctuations and the band operators associated with the X electron pocket can be obtained from:

$$H_{\text{int}, X} = \lambda \sum_{\mathbf{k}, \mathbf{k}'} \phi_{\mathbf{k}-\mathbf{k}'} \left(\cos \chi d_{yz, \mathbf{k}'}^\dagger d_{yz, \mathbf{k}} + \sin \chi d_{xy, \mathbf{k}'}^\dagger d_{xy, \mathbf{k}} \right) \quad (\text{S36})$$

$$H_{\text{int}, X} = \lambda \sum_{\mathbf{k}, \mathbf{k}'} \phi_{\mathbf{k}-\mathbf{k}'} \left(\frac{\alpha^2 \sin \chi + \cos \chi \sin \theta \sin \theta'}{\sqrt{(\alpha^2 + \sin^2 \theta')(\alpha^2 + \sin^2 \theta)}} \right) f_X^\dagger(\theta') f_X(\theta) \quad (\text{S37})$$

where $\chi = \tan^{-1}(\lambda_2/\lambda_1)$ and $\lambda = \sqrt{\lambda_1^2 + \lambda_2^2}$ are related to the two nematic couplings λ_1 and λ_2 . Since we are interested on the states at the Fermi level, we hereafter focus only on the contributions arising from bilinear combinations of f_X and f_Y , since the band dispersions corresponding to f'_X and f'_Y do not cross the Fermi surface. Similarly, for pocket Y we find:

$$H_{\text{int}, Y} = -\lambda \sum_{\mathbf{k}, \mathbf{k}'} \phi_{\mathbf{k}-\mathbf{k}'} \left(\frac{\alpha^2 \sin \chi + \cos \chi \cos \theta \cos \theta'}{\sqrt{(\alpha^2 + \cos^2 \theta')(\alpha^2 + \cos^2 \theta)}} \right) f_Y^\dagger(\theta') f_Y(\theta) \quad (\text{S38})$$

The linearized gap equations for the two pockets then become:

$$\eta \Delta_X(\theta) = \lambda^2 \chi_{\text{nem}} N_0 \ln \frac{\Lambda}{T} \int \frac{d\theta'}{2\pi} \frac{(\alpha^2 \sin \chi + \cos \chi \sin \theta \sin \theta')^2}{(\alpha^2 + \sin^2 \theta')(\alpha^2 + \sin^2 \theta)} \Delta_X(\theta'), \quad (\text{S39})$$

$$\eta \Delta_Y(\theta) = \lambda^2 \chi_{\text{nem}} N_0 \ln \frac{\Lambda}{T} \int \frac{d\theta'}{2\pi} \frac{(\alpha^2 \sin \chi + \cos \chi \cos \theta \cos \theta')^2}{(\alpha^2 + \cos^2 \theta')(\alpha^2 + \cos^2 \theta)} \Delta_Y(\theta'), \quad (\text{S40})$$

where Λ is the high energy cutoff, and N_0 is the density of states. These gap equations can be conveniently parametrized and solved in terms of the intra-orbital gaps Δ_1 and Δ_2 :

$$\Delta_X(\theta) = \frac{\Delta_1 \alpha^2 + \Delta_2 \sin^2 \theta}{\alpha^2 + \sin^2 \theta} \quad (\text{S41})$$

$$\Delta_Y(\theta) = \frac{\Delta_1 \alpha^2 + \Delta_2 \cos^2 \theta}{\alpha^2 + \cos^2 \theta} \quad (\text{S42})$$

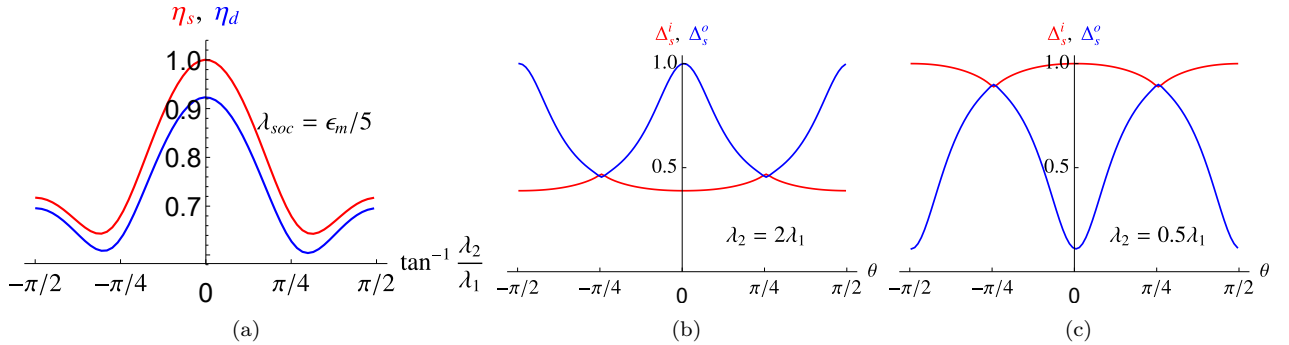


FIG. S7: SC in different channels for $\alpha = 0.5$ and $\lambda_{\text{SOC}} = 5\epsilon_m$. (a) The eigenvalues of the A_{1g} (s -wave) and B_{2g} (d -wave) pairing channels. (b) and (c): Projected gap functions of the A_{1g} solution onto the inner and outer electron pockets for $\lambda_2 = 2\lambda_1$ and $\lambda_2 = 0.5\lambda_1$, respectively.

To calculate the gap function in the presence of SOC and ISB, we need to write down the two additional non-interacting terms in the band basis. The SOC is given by

$$H_{\text{SOC}} = \frac{i}{2} \lambda_{\text{SOC}} \sum_{\mathbf{k}} \left[d_{xz, \mathbf{k}+\mathbf{Q}_Y}^\dagger \sigma_1 d_{xy, \mathbf{k}+\mathbf{Q}_X} + d_{xy, \mathbf{k}+\mathbf{Q}_Y}^\dagger \sigma_2 d_{yz, \mathbf{k}+\mathbf{Q}_X} \right] + h.c. \quad (\text{S43})$$

Projecting onto the Fermi surface, we find:

$$H_{\text{SOC}} = \lambda_{\text{SOC}} \sum_{\mathbf{k}} \frac{\alpha}{2\sqrt{\alpha^2 + \cos^2 \theta} \sqrt{\alpha^2 + \sin^2 \theta}} f_Y^\dagger (\cos \theta \sigma_1 - \sin \theta \sigma_2) f_X + h.c. \quad (\text{S44})$$

Similarly, the ISB term is:

$$H_{\text{ISB}} = \lambda_{\text{ISB}} \sum_{\mathbf{k}} d_{xz, \mathbf{k}+\mathbf{Q}_Y}^\dagger d_{yz, \mathbf{k}+\mathbf{Q}_X} + h.c. \quad (\text{S45})$$

whose projection onto the Fermi surface gives:

$$H_{\text{ISB}} = -\lambda_{\text{ISB}} \sum_{\mathbf{k}} \frac{\sin \theta \cos \theta}{\sqrt{\alpha^2 + \cos^2 \theta} \sqrt{\alpha^2 + \sin^2 \theta}} f_X^\dagger f_Y + h.c. \quad (\text{S46})$$

The results for the case of SOC are shown in Fig. S7 (for $\lambda_{\text{SOC}} \ll \epsilon_m$) and S8 (for $\lambda_{\text{SOC}} \gg \epsilon_m$). In the former case, the angular dependence of the gap functions in the inner and outer pockets, and the splitting of the A_{1g} and B_{2g} degeneracies, are similar to Fig. 2 of the main text, which was obtained using the full orbital model. In the latter case, the degeneracy lifting is more pronounced, and the gaps in the two pockets are similar, as shown in Fig. 4 of the main text.

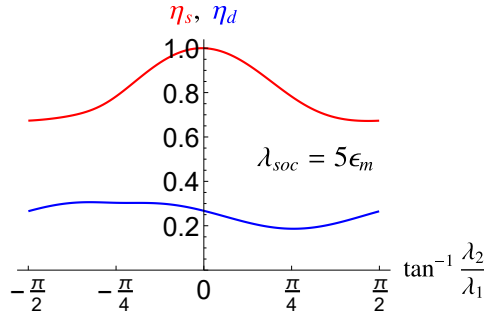


FIG. S8: Eigenvalues of the A_{1g} (s -wave) and B_{2g} (d -wave) pairing channels for $\alpha = 0.5$ and $\lambda_{\text{SOC}} = 5\epsilon_m$.

The impact of ISB on SC is similar to the case of SOC. As shown in Fig. S9 (for $\lambda_{\text{ISB}} \gg \epsilon_m$), the $A_{1g} + A_{2u}$ (s -wave) pairing is the leading instability. The angular dependence of the SC gap is also similar to the case of large SOC. The sharp peaks or troughs at $\theta = 0$ and $\pm\pi/2$ are a consequence of the fact that the effective ISB term λ_{ISB} vanishes at these points of the Fermi surface.

* Electronic address: jkang@umn.edu

[S1] V. Cvetkovic and O. Vafek, Phys. Rev. B **88**, 134510 (2013).

[S2] J. Kang, A. F. Kemper, and R. M. Fernandes, Phys. Rev. Lett. **113**, 217001 (2014).

[S3] S. V. Borisenko, *et al.*, Nat. Phys. **12** 311 (2016).

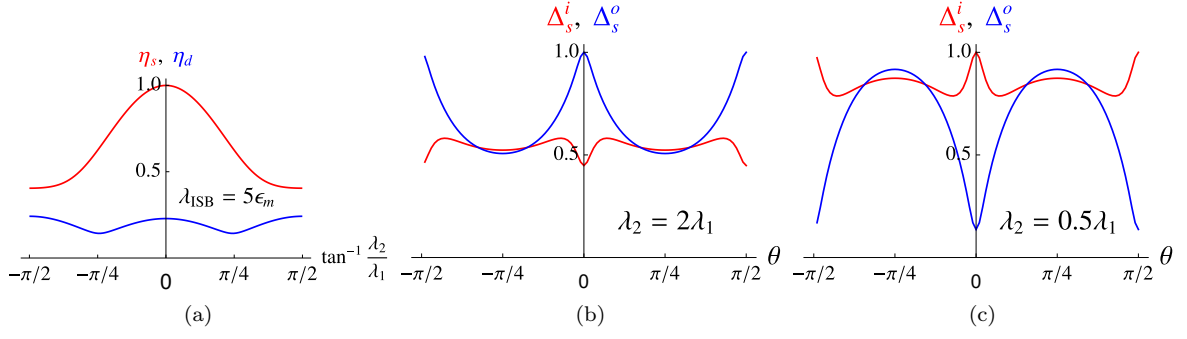


FIG. S9: SC in different channels for $\alpha = 0.5$ and $\lambda_{\text{ISB}} = 5\epsilon_m$. (a) The eigenvalues of the $A_{1g} + A_{2u}$ (s -wave) and B_{2g} (d -wave) pairing channels. (b) and (c): Projected gap functions of the $A_{1g} + A_{2u}$ solution onto the inner and outer electron pockets for $\lambda_2 = 2\lambda_1$ and $\lambda_2 = 0.5\lambda_1$, respectively.